NANO LETTERS

2008
Vol. 8, No. 8
2356-2361

# Spin-Dependent Tunneling Transport into $CrO_2$ Nanorod Devices with Nonmagnetic Contacts

**Yipu Song, Andrew L. Schmitt, and Song Jin***

*Department of Chemistry, University of Wisconsin-Madison, Madison, Wisconsin 53706*

*Received January 6, 2008; Revised Manuscript Received April 25, 2008*

## ABSTRACT

**Single-crystal nanorods of half-metallic chromium dioxide ($CrO_2$) were synthesized and structurally characterized. Spin-dependent electrical transport was investigated in individual $CrO_2$ nanorod devices contacted with nonmagnetic metallic electrodes. Negative magnetoresistance (MR) was observed at low temperatures due to the spin-dependent direct tunneling through the contact barrier and the high spin polarization in the half-metallic nanorods. The magnitude of this negative magnetoresistance decreases with increasing bias voltage and temperature due to spin-independent inelastic hopping through the barrier, and a small positive magnetoresistance was found at room temperature. It is believed that the contact barrier and the surface state of the nanorods have great influence on the spin-dependent transport limiting the magnitude of MR effect in this first attempt at spin filter devices of $CrO_2$ nanorods with nonmagnetic contacts.**

Highly spin polarized materials are extremely valuable to the fundamental studies and practical applications of spintronics, which seeks to exploit the spin properties instead of or in addition to charge degrees of freedom in electronic and photonic devices.[1–3] Ferromagnetic chromium dioxide ($CrO_2$) with a high Curie temperature ($T_c$) of 395 K has been predicted to be half-metallic on the basis of band structure calculations.[4,5] A half-metal is defined as a fully spin polarized material with majority spin electrons in metallic bands, while the minority spin electrons exist in a sub-band with a semiconductor like energy gap at the Fermi level.[6] A high degree of spin polarization ($\geq$95%) has indeed been experimentally demonstrated for $CrO_2$ using spin-polarized photoemission[7] and superconducting point-contact experiments.[8] This nearly perfect spin polarization suggests that $CrO_2$ would be ideal for spintronics, especially in spin filter applications. The half-metallic nature of $CrO_2$ has motivated intensive studies of their magnetoresistance properties,[9–11] intergranular tunneling,[12–14] and magnetic tunnel junction (MTJ) devices [15–17] using $CrO_2$ films and powder compacts. But in general, the material quality (crystallinity and purity) and its integration with other materials have been rather challenging.

One dimensional (1D) nanostructures have demonstrated their potential as building blocks for nanoelectronics[18–20] and begun to emerge as building blocks for nanospintronics as well.[21,22] Spin transport in ferromagnetic nanostructures is of fundamental interest in mesoscopic physics and unique properties could arise from shape anisotropy and low dimensionality. Large magnetoresistance effects (MR) are expected in ferromagnetic nanocontacts due to the nonadiabatic spin scattering across very narrow magnetic domain walls trapped at nanosized constrictions in the ballistic transport regime.[23] We are most interested in exploring the spin transport in nanowire/nanorod structures of *concentrated* magnetic semiconductors such as EuO,[24,25] $Fe_xCo_{1-x}Si$,[26,27] and $CrO_2$. Another interesting half-metallic oxide is magnetite ($Fe_3O_4$) though its half-metallicity is still somewhat controversial.[28] Other researchers have reported the synthesis and the basic transport properties of $Fe_3O_4$ nanowires,[29–31] but the spin transport in half-metallic nanostructures remains largely unexplored. High-quality single crystal nanoscale building blocks of $CrO_2$ could improve the device performance and relax the many material integration constraints based on traditional top-down device fabrication. In this letter, we report the synthesis, structural characterization, and the spin-dependent electrical transport of individual $CrO_2$ nanorods contacted with nonmagnetic metallic electrodes.

It has been known that it is difficult to prepare pure $CrO_2$ because it is a metastable phase at room temperature and ambient pressure,[6] though acicular $CrO_2$ is in fact industrially prepared for use in high end magnetic tape media. To overcome this difficulty and obtain high quality $CrO_2$ for device work, various methods have been developed. For example, epitaxial $CrO_2$ thin films have been grown on $TiO_2$ and $Al_2O_3$ substrates by chemical vapor deposition (CVD)

* To whom correspondence should be addressed. E-mail: jin@chem.wisc.edu.

10.1021/nl080038q CCC: $40.75 
**Published on Web 07/11/2008**

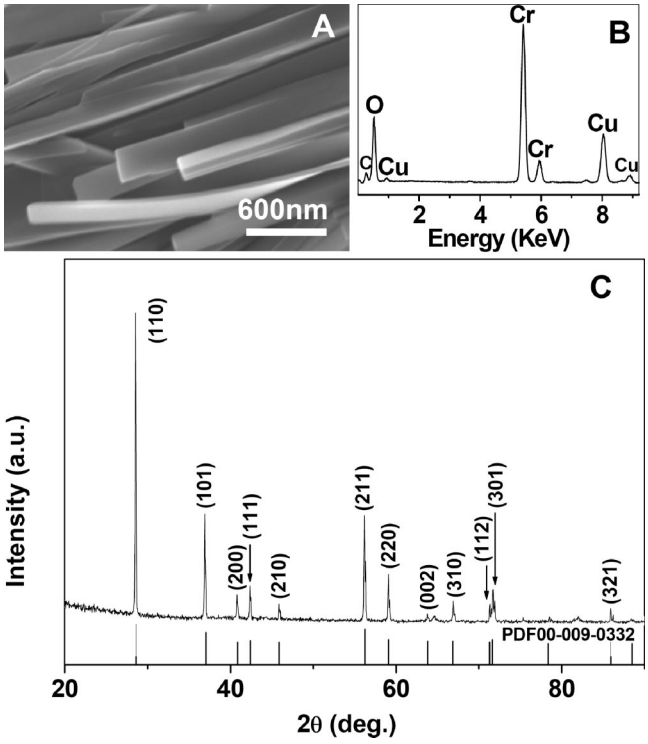


**Figure 1.** (A) Representative SEM image of the $CrO_2$ nanorods; (B) EDS spectrum recorded from a single nanorod (the Cu signal comes from the TEM grid); (C) powder X-ray diffraction pattern for a sample of $CrO_2$ nanorods.

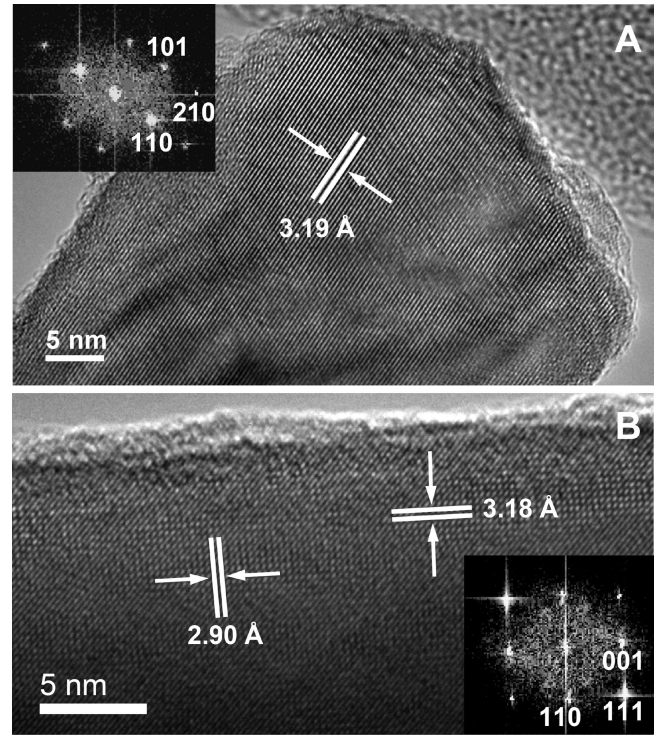


**Figure 2.** High-resolution TEM (HRTEM) images of representative $CrO_2$ nanorods with different growth axes. The images clearly show lattice fringes of the single-crystal rods with the [101] growth axis in panel A and [001] *c*-axis orientation in panel B. The insets show the indexed two-dimensional fast Fourier transform (FFT) of the lattice resolved images.

using $CrO_3$ or $CrO_2Cl_2$ as precursors.[32–34] We used a two-step method to synthesize pure $CrO_2$ nanorod samples similar to a simple route reported by Bajpai and Nigam.[35] First, $CrO_3$ powder (Alfa Aesar, 99.99%) was heated for 10 h at a temperature of 250 °C under ambient pressure and oxygen flow (100 sccm) to prepare an intermediate precursor oxide. Then 0.30 g of this precursor is sealed in a glass tube (I.D., 4.5 mm; length, 4 cm) at ambient pressures and heated at 393 °C for 2.5 h in a preheated furnace to yield the desired black product of $CrO_2$ nanorods in bulk quantity. Variations in experimental conditions lead to the formation of undesirable impurities in the final products. The key to produce pure $CrO_2$ phase, which is metastable in air, is to maintain a suitable overpressure of oxygen (that comes from the decomposition of higher Cr oxides). Therefore the size of the sealed tube is rather important and the reported conditions were empirically found to be effective. Pure $CrO_2$ only forms in the specified temperature window, between 392 and 396 °C. Either $Cr_2O_5$ or $Cr_2O_3$ impurity are observed in the samples on the lower-temperature or higher-temperature side of this optimal window, respectively.

This product contains mostly short nanorods. The morphology of the as-synthesized product was examined using field emission scanning electron microscopy (SEM, LEO SUPRA 1530). A representative SEM image (Figure 1A) reveals needle-shaped nanorods of mostly 30∼100 nm in diameter and 1∼2 $\mu$m in length. Larger sized rods with typical diameters of 400∼600 nm and lengths of 4∼5 $\mu$m were formed in the other variations of experimental conditions. The final product morphology (aspect ratio and rod size) depends on the mass of the precursor, the size of the glass tube, and the temperature and time taken for converting the specified amount of the precursor to $CrO_2$.

The bulk quantity of the nanorods produced readily allowed for phase characterization of the product using powder X-ray diffraction (PXRD), as shown in Figure 1C. All major diffraction peaks can be matched to that of the tetragonal structure of $CrO_2$ (JCPDS PDF00−009−0332) (Space group $P4_2/mnm$, No. 136, Person symbol *tP*6, rutile structural type). No other chromium oxide impurity phases are detectable by PXRD. The calculated lattice parameters from PXRD data: $a = 4.421$ Å, $c = 2.916$ Å are in good agreement with the literature.[36] The chemical composition of the nanorods was analyzed by energy-dispersive spectroscopy (EDS, Figure 1B), which reveals that the nanorod consists of Cr and O elements in the atomic ratios of Cr/O = 1:1.96. This is close to the chemical stoichiometry ratio for $CrO_2$ within the typical error of the method. EDS analysis at different positions of the nanorods show no noticeable change in compositions.

The $CrO_2$ nanorods were further characterized using transmission electron microscopy (TEM). The as-grown nanorods were sonicated at high power (to break up agglomeration driven by ferromagnetic ordering) and suspended in ethanol, dispersed onto TEM grids with lacey carbon film and imaged with a Philips CM200 TEM with an accelerating voltage of 200 kV. Figure 2A,B shows the high-resolution TEM (HRTEM) images of the representative

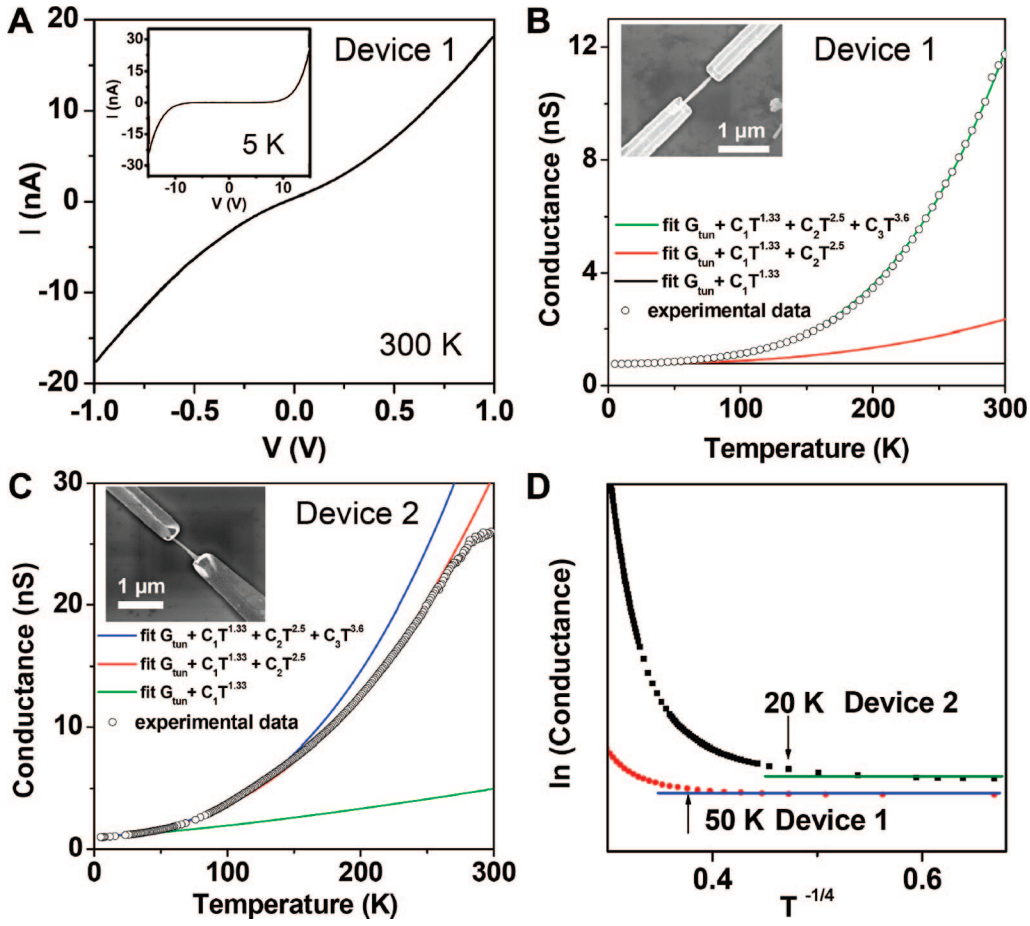


**Figure 3.** (A) Nonlinear current−voltage ($I-V$) characteristics recorded at 300 K and zero magnetic field for a representative two-terminal $CrO_2$ nanorod device (device 1) contacted with nonmagnetic metal electrodes. The inset shows the current−voltage curve at 5 K. (B,C) The conductance $G$ as a function of temperature for device 1 and device 2. The theoretical fits of $G$ as a function of $T$ obtained from the equation $G = G_{tun} + C_1T^{1.33} + C_2T^{2.5} + C_3T^{3.6}$ for device 1 with $C_1/C_2/C_3 = 1.2 \times 10^{-6}$:1:0.012 (panel B) and $G = G_{tun} + C_1T^{1.33} + C_2T^{2.5} + C_3T^{3.6}$ for device 2 with $C_1/C_2/C_3 = 1{:}8.3 \times 10^{-3}{:}5.0 \times 10^{-6}$ (panel C) are overlaid. At low temperatures, $G$ is mainly decided by the tunneling term; at high temperatures, $G$ is dominated by higher-order hopping that follows a power law. (Insets) SEM images of the measured devices. (D) ln $G$ plotted as $T^{-1/4}$ in the temperature range from 120 to 5 K showing the temperature independence of device conductance in the low temperature regime.

$CrO_2$ nanorods with different growth axes. The images clearly show lattice fringes of single-crystal $CrO_2$ rods with about 30 nm diameter along the [101] growth axis in Figure 2A and [001] $c$-axis orientation in Figure 2B. The two-dimensional fast Fourier transform (FFT) of the lattice-resolved images (insets of Figure 2A,B) show the reciprocal lattice peaks, which can be indexed to a primitive tetragonal lattice. The measured lattice spacing observed in HRTEM of Figure 2A is 3.19 Å, corresponding well to the (110) lattice spacing (3.125 Å) of the tetragonal $CrO_2$ structure. The measured lattice spacings of 2.90 and 3.18 Å (in Figure 2B) correspond to the (001) (2.915 Å) and (110) (3.125 Å) lattice spacings, respectively. It has been reported that a very thin naturally formed oxide layer of $Cr_2O_3$ with thickness of 1∼3 nm is always on the surface of $CrO_2$.[14] This thin amorphous layer (about 1 nm) was also observed for our samples.

To investigate the spin-dependent transport of single crystal $CrO_2$ nanorods with nonmagnetic contacts, two-terminal devices were fabricated using standard e-beam lithography. The nanorods were suspended in ethanol via ultrasonication and deposited onto degenerately doped Si/$SiO_2$ (600 nm) substrates. For making electrical contact to the nanorods, the samples are first treated with oxygen plasma (100 W) for 1 min to remove the organic contaminants from the nanorod surface, etched in concentrated (37 wt %) HCl solution for 20 s to remove the surface oxide layer, rinsed in DI water for 10 s, and then dried in a nitrogen flow prior to deposition of the 40 nm Ti and then 40 nm Au electrodes by e-beam evaporation. The electrical transport was carried out in Quantum Design Physical Property Measurement System (PPMS) using a Keithley 2400 source-meter under two-probe configuration. A dozen devices were investigated to different level of details with qualitatively similar device behavior. Data from three representative devices, named device 1 to 3, are discussed and shown in details herein. Figure 3A shows the current ($I$)−voltage ($V$) curve of a representative $CrO_2$ nanorod device (device 1) at temperature 300 K and the inset shows the $I-V$ curve measured at 5 K. The $I-V$ curve is nonlinear at room temperature and becomes more nonlinear at low temperatures. Nonlinear $I-V$ curves indicate the barrier's contribution to electrical transport. As the bias voltage increases

above the barrier height, the current increases rapidly. The formation of the barrier is mostly due to the thin impurity oxide layer on the $CrO_2$ surface, such as $Cr_2O_3$, which is an antiferromagnetic insulator ($T_N = 307.6$ K), as well as the different work functions between metal electrode and the ferromagnetic nanorod. Even though we purposefully employed an HCl acid etching step before making contact, it is possible that the etching process does not completely remove the oxide layer or new impurity oxide layer can form at the interface between Ti metal and $CrO_2$, which is reasonable thermodynamically.

The temperature dependence of the conductance can provide insight into the nature of the transport properties of the devices. The conductance is measured with a constant current when the device is cooling down from 300 to 5 K. Figure 3B,C shows the temperature dependent conductance ($G$) of two devices (device 1 and device 2) while the insets show the SEM images of the particular devices. The currents used for the measurements were 10 nA for device 1 and 6 nA for device 2. The device conductance decreases with the decrease of the temperature by a factor of 15 and 30 in the temperature range from 300 to 5 K for device 1 and device 2, respectively. Previous studies on magnetic tunnel junctions based on the $CrO_2$ film and intergranular tunneling based on the $CrO_2$ powder show similar temperature dependence, i.e., the conductance decreases with decreasing temperature.[13–16] But for the pure $CrO_2$ films, the conductivity was reported to increase with decreasing temperature.[5,9,10] This difference clearly shows that the barrier plays a crucial role in the conduction transport of our devices. One can also see that there is a significant slope change in conductance starting from about 50 K for device 1 and 20 K for device 2 and the conductance is almost temperature independent for both devices at low temperature. In order to show this more clearly, the ln $G$ is plotted against $T^{-1/4}$ in Figure 3D in the temperature range from 120 to 5 K. It is apparent that the conductance is temperature independent from temperature range 5−50 K for device 1 and 5−20 K for device 2. This temperature independence is indicative of elastic direct tunneling at low temperatures,[37] which is different from the variable range hopping ($T^{-1/4}$ dependence) and intergranular tunneling ($T^{-1/2}$ dependence),[13,37] which is neither expected, based on the single-crystalline nature of the $CrO_2$ nanorods, nor observed. This elastic tunneling is a spin-dependent process. However, when $T > 50$ K for device 1 and $T > 20$ K for device 2, the ln $G$ starts to deviate from the independent behavior, which suggests other mechanisms may become dominant at high temperature. It is known that, besides the direct elastic tunneling, phonon-assisted inelastic hopping processes through several localized states in the barriers can quickly dominate the tunneling conductance with increasing temperature, resulting in a temperature-dependent and spin-independent conductance. According to the analysis of Glazman et al.[38] and Xu et al.,[37] the inelastic hopping conductance has a power-law temperature dependence, $G_N^{hop} = T^{N-[2/(N+1)]}$,[13] where $N$ is the number of the localized states and the order of electron inelastic hopping. The order of electron inelastic hopping $N$ can be increased by increasing temperature and bias voltage. Thicker barriers can also result in a higher order of inelastic hopping, which is associated with an increased the number of localized states. The conductance of our devices can be fitted quite well by $G = G_{tun} + C_1T^{1.33} + C_2T^{2.5} + C_3T^{3.6}$, as shown in Figure 3B,C. The first term ($G_{tun}$) represents the spin-dependent tunneling channel. The second, third, and fourth terms represent the spin-independent channel of the power-law $T^{\delta}$ with $\delta = N-[2/(N+1)] = 1.33$ ($N = 2$, second-order hopping), 2.5 ($N = 3$, third-order hopping) and 3.6 ($N = 4$, fourth-order hopping), respectively. It is found for device 1 that the $T^{3.6}$ term is non-negligible and the transport is dominated by the fourth-order hopping term ($T^{3.6}$) and third-order hopping term ($T^{2.5}$). The second-order hopping ($T^{1.33}$ with $N = 2$) does not significantly contribute to the transport for this device. However for device 2, the $T^{3.6}$ term can be neglected and the hopping conductance is dictated by the lower order hopping ($T^{2.5}$ term and $T^{1.33}$ term). The theoretical investigation by Xu et al. [37] predicts that, as the barrier thickness increases, hopping chains with more than two localized states play a more important role. The increase of hopping order and the absence of $T^{1.33}$ term for device 1 are likely due to the higher barrier thickness. This is consistent with the fact that device 2 is more conductive than device 1. It is reasonable to believe that the higher effective barrier thickness for device 1 dominates the conductance measurement. This inelastic hopping through the barrier seems to work well in describing the observed transport phenomena.

The magnetoresistance (MR) measurements were conducted with a constant bias voltage and a magnetic field applied perpendicular to the substrate (transverse MR). The MR is defined as $MR = [R(H) - R(0)]/R(0)$, where $R(H)$ and $R(0)$ are the resistance at an applied field (up to 9 T) and zero field, respectively. The bias voltages used for the measurements were 12 V for device 1 and 6 V for device 2, respectively. Figure 4A shows the transverse MR curves for device 1 at 300 and 5 K, respectively. At room temperature, the transverse MR is small and positive (1.3%); however, negative MR was found at low temperature (5 K) and reaches 9.7% at 9 T. Similar MR behavior is observed for device 2: a negative MR (6.0%) was found at 5K, which decreases with increasing temperature to only negative 1.1% at 100 K. At room temperature, there is only an intrinsic positive MR (3.3%). Measurements on five other devices also show similar MR behavior. In previous studies of the MR properties of $CrO_2$ thin films,[9,10] Suzuki and Tedrow reported negative transverse MR in the temperature range from 360 to 4.2 K but the magnitude of the MR decreases as the field increases in the higher field range.[10] Watts et al. found a positive MR at low temperature and a small negative MR at high temperature with transverse magnetic field.[9] Despite the different MR results, the resistance of $CrO_2$ film decreases with temperature for both of these two cases. However, the temperature dependence of the resistance observed for our devices is in contradiction to their results, which further indicates that the barriers play crucial roles in conduction transport and the MR mechanism should be different from those cases.

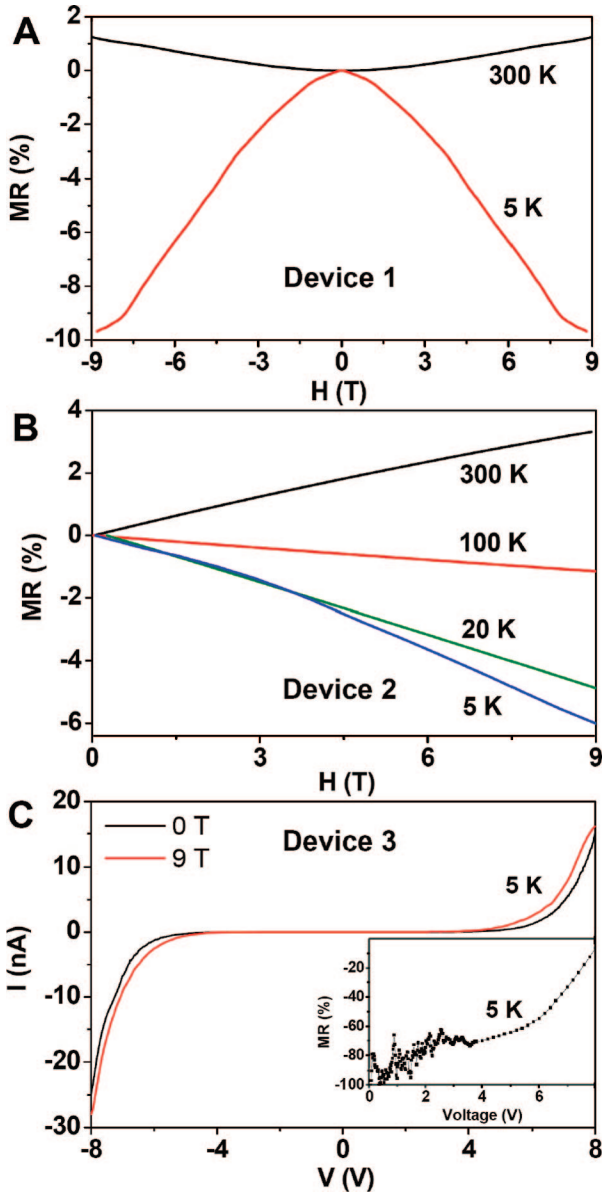


**Figure 4.** Transverse magnetoresistance (MR) with magnetic field up to 9 T for device 1 (A) and device 2 (B). (C) Current−voltage characteristics for device 3 measured at 5 K at $H = 0$ T (black curve) and $H = 9$ T (red curve), respectively. The inset shows the bias dependence of the MR for this device.

Our $CrO_2$ nanorod device can be considered as a half-metallic nanorod sandwiched between two normal metal electrodes with contact barriers (Figure 5). Below the ferromagnetic ordering temperature ($T_c = 395$ K) of $CrO_2$, the Fermi level is located in a relatively narrow band (width less than 1 eV) of the majority electrons, and the minority-spin electrons have a bandgap of 1.5 eV, which means only the spin-up majority electrons can transport through the ferromagnetic nanorod. Hence, the ferromagnetic nanorods could act as an efficient spin filter on a traversing current; that is, the transverse component of spin angular momentum, which is filtered out of the current, must be absorbed by the half-metallic nanorod. The total device resistance comes from the two contact resistances and the nanorod resistance of which the nano-contact barrier dominates the spin-dependent transport. As

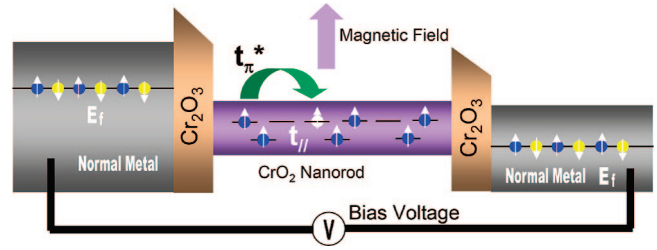


**Figure 5.** A schematic illustration of half-metallic $CrO_2$ nanorod device contacted with nonmagnetic metal electrodes with contact barriers.

mentioned before, an antiferromagnetic insulating layer, $Cr_2O_3$, is always naturally formed on the surface of $CrO_2$. Spin-resolved inverse photoemission investigations[39] indicate that the conduction band of $Cr_2O_3$ is polarized through antiferromagnetic coupling by the highly polarized ferromagnet, $CrO_2$.[40] This induced polarization, reflected in a minority spin asymmetry in the conduction band of $Cr_2O_3$, results in a net magnetic ordering at the surface of the insulating layer. The negative MR found in our devices at low temperature is likely due to the alignment of the induced polarization in the conduction band of $Cr_2O_3$ by the external magnetic field where $Cr_2O_3$ is serving as a quasimagnetic tunnel barrier.[41] The alignment of induced polarization reduces the scattering at the interface for the majority electrons that can only transport through the ferromagnetic nanorod. Although the $CrO_2$ nanorod has the intrinsic positive MR due to the cyclotron orbital motion of the conduction electrons, the negative MR effect of the contact resistance counteracts this small intrinsic positive MR at high field strengths. Therefore, the total device resistance shows negative MR behavior at low temperature. More spin-independent high-order inelastic tunneling channels will be open with increasing temperature, which would suppress the negative MR. Therefore the negative MR decreases with increasing temperature and only the intrinsic positive MR remains at room temperature. It is noteworthy that negative transverse MR is also expected in ferromagnetic systems when the mean free path of the charge carriers is of the same order of magnitude as the structure size.[42] Since the diameter of the nanorod is about 75 nm and the mean free path in $CrO_2$ is as large as 70 nm at 5 K,[5] this size effect is expected at low temperature. This could be another possible mechanism contributing to the negative MR observed in our devices.

The bias dependence of the magnetoresistance was also investigated for our devices. Figure 4C shows the current−voltage ($I-V$) curves for device 3 measured at 5 K with transverse magnetic fields of 0 T (black curve) and 9 T (red curve), respectively. The MR is derived from two $I-V$ curves according to MR $= [R(\mathrm{H}) - R(0)]/R(0)$. Although the MR data is noisy when the bias is below 4 V, it is clear to see that the negative MR decreases rapidly from 70% to 6% as the bias voltage increases from 4 to 8 V (Figure 4C inset). This bias dependence of MR could be attributed to the fact that the inelastic hopping through the contact barrier (vide supra) increases with increasing bias voltage, which results in the spin independent transport and suppresses the MR effect in the devices.[37,38]

In conclusion, we have studied the spin-dependent tunneling transport in single-crystal $CrO_2$ nanorod devices contacted with nonmagnetic metal electrodes. Negative magnetoresistance was observed at low temperature, which is attributed to spin-dependent tunneling through the contact barriers that are polarized by the half-metallic $CrO_2$ nanorods. The magnitude of the magnetoresistance decreases rapidly with increasing temperature and bias voltage, which is attributed to spin-independent inelastic hopping through contact barriers. It is believed that this contact barrier and the surface state of the nanorods have great influence on the spin-dependent transport in $CrO_2$ nanorod devices limiting the magnitude of MR in these spin filter devices. Further improvement over the barriers by development of better surface treatment and the selection of more appropriate (noble and inert) metal electrodes are expected to increase the device performance.

**Acknowledgment.** This research was supported by Research Corporation through a Cottrell Scholar Award to S.J., a Draper TIF grant, and the startup fund provided by UW-Madison. S.J. also thanks NSF (CAREER DMR-0548232), 3M Nontenured Faculty Award, and DuPont Young Professor Grant for support. We thank Professor Robert J. Hamers for the access to SEM and Professor Mark Eriksson for access to the PPMS.

**Supporting Information Available:** This material is available free of charge via the Internet at http://pubs.acs.org.

## References

(1) Zutic, I.; Fabian, J.; Das Sarma, S. *Rev. Mod. Phys.* **2004**, *76*, 323.
(2) Wolf, S. A.; Awschalom, D. D.; Buhrman, R. A.; Daughton, J. M.; Von Molnar, S.; Roukes, M. L.; Chtchelkanova, A. Y.; Treger, D. M. *Science* **2001**, *294*, 1488.
(3) Von Molnar, S.; Read, D. *Proc. IEEE* **2003**, *91*, 715.
(4) Schwarz, K. *J. Phys. F* **1986**, *16*, L211.
(5) Lewis, S. P.; Allen, P. B.; Sasaki, T. *Phys. Rev. B* **1997**, *55*, 10253.
(6) Coey, J. M. D.; Venkatesan, M. *J. Appl. Phys.* **2002**, *91*, 8345.
(7) Dedkov, Y. S.; Fonine, M.; Konig, C.; Rudiger, U.; Guntherodt, G.; Senz, S.; Hesse, D. *Appl. Phys. Lett.* **2002**, *80*, 4181.
(8) Ji, Y.; Strijkers, G. J.; Yang, F. Y.; Chien, C. L.; Byers, J. M.; Anguelouch, A.; Xiao, G.; Gupta, A. *Phys. Rev. Lett.* **2001**, *86*, 5585.
(9) Watts, S. M.; Wirth, S.; von Molnar, S.; Barry, A.; Coey, J. M. D. *Phys. Rev. B* **2000**, *61*, 9621.
(10) Suzuki, K.; Tedrow, P. M. *Phys. Rev. B* **1998**, *58*, 11597.
(11) Keizer, R. S.; Goennenwein, S. T. B.; Klapwijk, T. M.; Miao, G.; Xiao, G.; Gupta, A. *Nature* **2006**, *439*, 825.
(12) Coey, J. M. D.; Berkowitz, A. E.; Balcells, L.; Putris, F. F.; Barry, A. *Phys. Rev. Lett.* **1998**, *80*, 3815.
(13) Dai, J.; Tang, J. *Phys. Rev. B* **2001**, *63*, 054434.
(14) Dai, J. B.; Tang, J. K.; Xu, H. P.; Spinu, L.; Wang, W. D.; Wang, K. Y.; Kumbhar, A.; Li, M.; Diebold, U. *Appl. Phys. Lett.* **2000**, *77*, 2840.
(15) Parker, J. S.; Ivanov, P. G.; Lind, D. M.; Xiong, P.; Xin, Y. *Phys. Rev. B* **2004**, *69*, 220413.
(16) Miao, G. X.; Leclair, P.; Gupta, A.; Xiao, G.; Varela, M.; Pennycook, S. *Appl. Phys. Lett.* **2006**, *89*, 022511.
(17) Gupta, A.; Li, X. W.; Xiao, G. *Appl. Phys. Lett.* **2001**, *78*, 1894.
(18) Zhong, Z.; Wang, D.; Cui, Y.; Bockrath, M. W.; Lieber, C. M. *Science* **2003**, *302*, 1377.
(19) Li, Y.; Qian, F.; Xiang, J.; Lieber, C. M. *Mater. Today* **2006**, *9*, 18.
(20) Thelander, C.; Agarwal, P.; Brongersma, S.; Eymery, J.; Feiner, L. F.; Forchel, A.; Scheffler, M.; Riess, W.; Ohlsson, B. J.; Goesele, U.; Samuelson, L. *Mater. Today* **2006**, *9*, 28.
(21) Hueso, L. E.; Pruneda, J. M.; Ferrari, V.; Burnell, G.; Valdes-Herrera, J. P.; Simons, B. D.; Littlewood, P. B.; Artacho, E.; Fert, A.; Mathur, N. D. *Nature* **2007**, *445*, 410.
(22) Kulkarni, J. S.; Kazakova, O.; Holmes, J. D. *Appl. Phys. A* **2006**, *85*, 277.
(23) Chopra, H. D.; Hua, S. Z. *Phys. Rev. B* **2002**, *66*, 020403.
(24) Bierman, M. J.; Van Heuvelen, K. M.; Schmeisser, D.; Brunold, T. C.; Jin, S. *Adv. Mater.* **2007**, *19*, 2677.
(25) Wachter, P. Europium chalcogenides: EuO, EuS, EuSe and EuTe. In *Handbook on the physics and chemistry of rare earths*; Gschneide, K. A., Jr.; Eyring, L., Eds.; North-Holland: Amsterdam, 1979; Vol. 2, pp 507−574..
(26) Schmitt, A. L.; Higgins, J. M.; Jin, S. *Nano Lett.* **2007**, *8*, 810.
(27) Manyala, N.; Sidis, Y.; DiTusa, J. F.; Aeppli, G.; Young, D. P.; Fisk, Z. *Nature* **2000**, *404*, 581.
(28) Tobin, J. G.; Morton, S. A.; Yu, S. W.; Waddill, G. D.; Schuller, I. K.; Chambers, S. A. *J. Phys.: Condens. Matter* **2007**, *19*, 315218.
(29) Zhang, D. H.; Liu, Z. Q.; Han, S.; Li, C.; Lei, B.; Stewart, M. P.; Tour, J. M.; Zhou, C. W. *Nano Lett.* **2004**, *4*, 2151.
(30) Liao, Z. M.; Li, Y. D.; Xu, J.; Zhang, J. M.; Xia, K.; Yu, D. P. *Nano Lett.* **2006**, *6*, 1087.
(31) Chang, M.-T.; Chen, L.-J.; Hsieh, C.-H.; Chueh, Y.-L.; Wang, Z. L.; Murakami, Y.; Shindo, D. *Adv. Mater.* **2007**, *19*, 2990.
(32) Li, X. W.; Gupta, A.; McGuire, T. R.; Duncombe, P. R.; Xiao, G. *J. Appl. Phys.* **1999**, *85*, 5585.
(33) Gupta, A.; Li, X. W.; Xiao, G. *J. Appl. Phys.* **2000**, *87*, 6073.
(34) Gupta, A.; Li, X. W.; Guha, S.; Xiao, G. *Appl. Phys. Lett.* **1999**, *75*, 2996.
(35) Bajpai, A.; Nigam, A. K. *Appl. Phys. Lett.* **2005**, *87*, 222502.
(36) Thamer, B. J.; Douglass, R. M.; Staritzky, E. *J. Am. Chem. Soc.* **1957**, *79*, 547.
(37) Xu, Y.; Ephron, D.; Beasley, M. R. *Phys. Rev. B* **1995**, *52*, 2843.
(38) Glazman, L. I.; Matveev, K. A. *Pis'ma Zh. Eksp. Teor. Fiz.* **1988**, *48*, 403.
(39) Cheng, R.; Komesu, T.; Jeong, H. K.; Yuan, L.; Liou, S. H.; Doudin, B.; Dowben, P. A.; Losovyj, Y. B. *Phys. Lett. A* **2002**, *302*, 211.
(40) Tiusan, C.; Greullet, F.; Hehn, M.; Montaigne, F.; Andrieu, S.; Schuhl, A. *J. Phys.: Condens. Matter* **2007**, *19*, 165201.
(41) Moodera, J.; Santos, T.; Nagahama, T. *J. Phys.: Condens. Matter* **2007**, *19*, 165202.
(42) Askerov, B. M.; Kuliev, B. I.; Shteinshraiber, V. Y. *Fiz. Tekh. Poluprovodn.* **1983**, *17*, 1701.

NL080038Q